GFRP Reinforced Bridge Barriers: Numerical Modeling

PREPARED BY:

Congjie Wei, M.S., Graduate Research Assistant

John Myers, Ph.D., Professor

Chenglin Wu, Ph.D., Assistant Professor

Missouri University of Science and Technology

PREPARED FOR:

Missouri Department of Transportation

Construction and Materials Division, Research Section

TECHNICAL REPORT DOCUMENTATION PAGE

1. Report No. cmr 22-009	2. Government Accession No.	3. Recipient's Catalog No.	
4. Title and Subtitle GFRP Reinforced Bridge Barriers: Numerical Modeling		**5. Report Date** August 2022 Published: August 2022	
		6. Performing Organization Code	
7. Author(s) Congjie Wei, M.S. John Myers, Ph.D. Chenglin Wu, Ph.D.		**8. Performing Organization Report No.**	
9. Performing Organization Name and Address Department of Civil, Architectural and Environmental Engineering Missouri University of Science and Technology 1401 N. Pine St., Rolla, MO 65409		**10. Work Unit No.**	
		11. Contract or Grant No. MoDOT project # TR202112	
12. Sponsoring Agency Name and Address Missouri Department of Transportation (SPR-B) Construction and Materials Division P.O. Box 270 Jefferson City, MO 65102		**13. Type of Report and Period Covered** Final Report (February 2021-August 2022)	
		14. Sponsoring Agency Code	

16. Abstract

The reported work enclosed the numerical modeling of GFRP reinforced concrete bridge barrier under static and impact load. The GFRP configurations were designed to fit into the existing MoDOT Type D barrier structures. The constructability of the GFRP reinforcement was also taken into consideration. Both static and dynamic loading were modeled to examine the strength of the GFRP reinforced concrete bridge barrier under vehicle impact. The results showed that the designed barrier can withhold a reaction force of 200 kips, which satisfies the AASHTO specifications. The design load is also significantly higher than the impact loads generated by vehicle collision.

17. Key Words Glass fiber reinforced polymer; Impact loads; Reinforced concrete bridges; Static loads	**18. Distribution Statement** No restrictions. This document is available through the National Technical Information Service, Springfield, VA 22161.		
19. Security Classif. (of this report) Unclassified.	**20. Security Classif. (of this page)** Unclassified.	**21. No. of Pages** 44	**22. Price**

GFRP Reinforced Bridge Barriers: Numerical Modeling

Project Number: TR202112

Final Report

Investigator

Dr. John Myers, Professor

Dr. Chenglin Wu, Assistant Professor

Missouri S&T

June 2022

COPYRIGHT

DISCLAIMER

ACKNOWLEDGMENTS

EXECUTIVE SUMMARY

The main objective of this research is to design a concrete barrier that is reinforced with glass fiber reinforced polymer (GFRP) materials. The design is based on the MoDOT Type D concrete barriers with steel bar reinforcements. The constructability of the GFRP reinforcement was also considered during the design process. This design adjusts the sizes and dimensions to match the properties of GFRP reinforcements. This exchange of the reinforcement materials is meant to take advantage of the preservative properties of GFRP materials to enhance the resistance to corrosion introduced degradation and damage.

The strength as well as the behavior of GFRP reinforced concrete barrier under different types of loadings is then explored and modeled using commercial software ABAQUS and LS-Dyna. The static loading is firstly applied to the GFRP and steel bar reinforced concrete barriers for comparison. Different concrete barrier models are also considered to study the influence of different cast approaches. Afterwards, the behaviors of GFRP reinforced concrete barriers under car and truck impact scenarios are also modeled. Simplified models as well as full size models are both studied using ABAQUS and LS-Dyna separately. Truck collisions with different angles are considered to explore the behavior of GFRP reinforced concrete barrier under different possible collision scenarios. The modeling results show that the reaction forces from the dynamic impact modeling are much lower than the design strength.

Keywords: GFRP reinforced concrete barrier, reinforcement design, static loading, impact study, finite element modeling

CONTENTS

LIST OF FIGURES

LIST OF TABLES

1. INTRODUCTION

1.1 Problem Statement

Concrete road barriers play an important role in protecting lives from injury or fatal damage and preventing vehicles from entering the opposite lane or other dangerous areas by dividing opposing lanes of many types of roads. Being the last protection after a vehicle loses control, the concrete barriers should be able to prevent the vehicle entering the opposite lane or steering into a field that would introduce more severe accidents than hitting the barrier. It is essential to understand the behavior and possible failure of the concrete barriers under different impact scenarios that comes with different types of vehicle and impact angles, among many factors that would influence the impact results. Moreover, current concrete barriers are mostly reinforced with steel bar, which has excellent strength that are validated with countless experiments and numerical analysis. One main disadvantage of this group of reinforced concrete is the corrosion introduced degradation and damage, which can be vastly improved by changing the reinforcement to non-corrosive high strength materials like glass fiber reinforced polymer (GFRP).

This project aims to provide a rational design of GFRP reinforced MoDOT Type D concrete bridge barriers that can withstand MASH loading. Different types of GFRP design for barrier and transverse bars in deck are proposed and designed based on literature survey and group discussions. A lot of research has been conducted to explore the safety of the bridge concrete barriers using experimental or numerical approaches. The NCHRP Report 350 [1] presented the experiment results of a series of crash test including multiple types of vehicles on different types of barriers. Elham, et al. [2] studied the behavior of steep curvature barriers under the truck impact with different self-weights and different velocities at collision. Results show that chances are the truck overriding the concrete barrier, depending mainly on the height of the barrier rather than the shape and effect of friction. This is also verified by other related research, Dhafer, et al. [3], Sheikh, et

al. [4] and Jeon, et al. [5] are among the works exploring the influence of barrier shapes on the safety using experimental approaches. Numerical approaches are also adopted to explore the key factors influencing the safety of concrete barriers and LS-Dyna is the most common software used in this process. Esfahani et al. [2] studied the F-shape and New Jersey concrete barriers using LS-Dyna. Similar works include Sturt and Fell [6] and Atahan [7].

Currently, the steel bar reinforcement is still the most used material in concrete structures. The superior mechanical properties of this type of structures have proved to be ideal for construction of large-scale buildings and structures. However, one main problem all steel bar reinforced concrete structures must face is the corrosion, which has emerged to be one of the most critical reliability issues of our crumbling civil infrastructure. Things could be even worse for structures under effect of seawater, frozen soil, or other corrosive environments. Each year, hundreds of billions of dollars are spent to deal with the corrosion related repair or maintenance projects. Furthermore, the corrosion introduced damage could lead to catastrophic failure of bridge structures, which could lead to loss of human lives as well. The corrosion process is triggered by the infusion of chloride and oxygen ions, which is enhanced by the porous solid nature of concrete materials. The electrode reactions at the interface between the reinforcement and concrete materials consumes the iron and produces ferric oxide, which is also known as rust. This electrochemical reaction production will lead to a volume expansion and further large stress concentrations in the reinforced concrete, which in turn introduces damages to the concrete and expanded the infusion channels for the chloride and oxygen ions from the environment. This process causes safety problems by degrading the reinforcement material strength as well as the bond strength between the reinforcements and concrete. Lots of research has also been conducted to understand this corrosion process at the interfaces of reinforcement and concrete to find a way for prediction and protection theoretically, numerically, and experimentally. F.Tondolo [8] studied

2

the bond strength change under different degree of corrosion. Wei et al. [9] developed a hydro-chemo-mechanical coupled phase field formulation to study the damage development in the reinforced concrete, which is among the multiple models that can be used for the corrosion prediction [10, 11]. Experimental approaches have also been adopted for this study, related works include Fernandez et al. [12], Hong et al. [13] and so on.

Being immune to the corrosive problems, glass fiber reinforced polymer (GFRP) reinforcement has recently drawn tremendous amount of interest in engineering practice. This class of materials could save tremendous efforts that are currently spent to deal with the corrosion related problems. Moreover, GFRP also has excellent mechanical properties. Being made from extremely fine fiber of glass, this group of material combines the high strength and stiffness of the glass fiber and the ductility of the soft resin, which makes it an ideal candidate for reinforcements of concrete structures. These advantages have attracted the focus of many researchers, related research projects include, [14-26]. These studies provide confidence to engineers for field implementation of GFRP in bridge structures. Since the first steel-free deck used by MoDOT in 2007, both Carbon Fiber Reinforced Polymer (CFRP) and Glass Fiber Reinforced Polymer (GFRP) bars have been used in 4-5 bridge decks on the state bridge system. These previous efforts along with the reduced prices have promoted potential implementation of both steel-free deck and barrier.

1.2. Research Objectives

This project aims to design a MoDOT Type D barrier that is reinforced with GFRP materials. To verify the safety and feasibility of this design, as well as understanding the performance of this GFRP reinforced concrete barrier under impact of different types of vehicles, static and dynamic finite element modeling cases are conducted with different commercial software including ABAQUS and LS-DYNA.

To fulfil the former mentioned objectives, the tasks of this project are summarized and present as follows,

Task 1: GFRP Reinforcement Design Based on a MoDOT Type D Barrier

The research team works closely with MoDOT's Bridge Division for the preliminary design of the GFRP reinforcement. Two preliminary design approaches are proposed here. The first one is the straight anchorage bar design based on the experimental results from Azimi et al. (2014) and Sennah and Hedjazi (2019). The GFRP bar configuration was designed to be able to fit in the MoDOT single-slope Type D barrier. The second one is the single-bend bar with closed stirrup based on the results from Rocchetti and Nanni et al. (2017). The detailed configuration of the GFRP reinforcement was also tailored to fit into the existing MoDOT Type D barrier. Finally, two other options will also be discussed with the project TAC prior to proceeding including those being considered in Florida and Ohio.

Task 2: Behavior of GFRP Reinforced Concrete Barrier Under Static Loading Conditions

Three-dimensional numerical models are constructed and analyzed based on commercial software ABAQUS. The loading area is designed based on the TL4-TL6 conditions as specified in the AASHTO / MoDOT specifications. The loading is gradually increased until the failure of the barrier to explore the damage mechanism that are defined by the reaction force, stress/damage distribution as well as the strength corresponding to the failure moment.

Task 3: Behavior of GFRP Reinforced Concrete Barrier Under Dynamic Loading Conditions

ABAQUS Explicit finite element modeling as well as the LS-dyna are used for the calculation of three-dimensional numerical models under impact test with different types of vehicles. AASHTO and MASH barrier testing standards are referred and adopted for guidance of the model

construction and modeling setups. Different impact angle is considered to simulate all possible impact scenarios in real world.

1.3. Research Methodology

The static and dynamic modeling tasks are carried out with 2 commercial software, ABAQUS and LS-Dyna.

1.3.1 ABAQUS

ABAQUS FAE is a software suite for finite element analysis and computer-aided engineering, originally released in 1978 and now widely used in automotive, aerospace, and industrial products industries as well as research. ABAQUS has the capability of wide material modeling, which makes it popular among non-academic and research institutions in engineering. The capability of multi-physics coupled modeling, including piezoelectric, thermal, acoustic et al., also expands its application in fields beyond mechanics and structural design. Moreover, this software allows users to design and simulate with their own material and element models so as to eliminate the limitations of implemented modulus.

1.3.2 LS-Dyna

LS-DYNA is an advanced general-purpose multi-physics simulation software package developed by the former Livermore Software Technology Corporation (LSTC). This software is mainly used for nonlinear simulations, including the changing boundary conditions, large deformation. This capability makes it ideal for simulations of automotive crashes.

2. RESEARCH PROGRAM (TASKS)

2.1 GFRP Reinforcement Design Based on a MoDOT D Type Barrier

The GFRP reinforced concrete barrier design is mainly based on the MoDOT Type D barrier design. The sizes and bends are adjusted to meet the requirements for glass fiber rebar specifications. The two-piece design is shown in Fig. 1. 2 stirrups are considered, stirrup 1 is a hooked bar that is designed mainly for the upper part strength of the barrier. Stirrup 2 is a closed stirrup to connect the barrier to the bridge deck. The stirrups are designed to have the minimum number of bends and a minimum radius of 2.5 inch and is satisfied for all positions. These stirrups are along the cross-section directions and aligned with a spacing of 6 inch. A total of 14 straight bars were aligned along the longitudinal direction of the barrier. The detail of the GFRP is based on two main factors: (1) to provide sufficient concrete cover when embedded into existing Type D barrier configuration; and (2) to satisfy the constructability. The research team has discussed with MoDOT engineers and industry collaborators. The proposed bent in both stirrups, especially stirrup 2, could be achieved by the mandrel fabrication process [27].
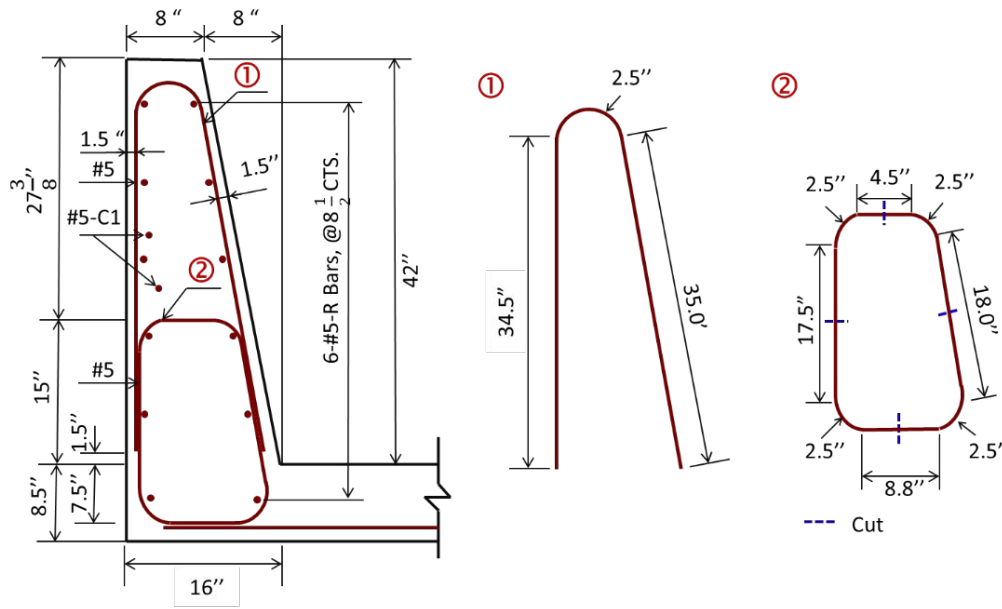

Figure 1 Two-piece GFRP reinforcement design details.

2.2 Behavior of GFRP Reinforced Concrete Barrier Under Static Loading Conditions

This work aims to provide quantitatively analysis and comparison between concrete bridge barriers reinforced with different types of materials (GFRP and steel bar) and different casting procedures (as a whole and separated). Parameter study is also conducted on the interspace (Δl=6, 9, 10, 12 *in*.) for all setups to explore the optimized reinforcement setup. All the cases studied in this part are carried out in commercial finite element software, ABAQUS.

2.2.1 Model Construction

A three-dimensional barrier with length of 17.5 ft, which is set to be 5 times of the loading area width to reduce the boundary effect, is constructed and used for static loading modeling, as shown in Fig. 2. The cross-section follows the type D barrier of the ASSHTO code while the reinforcement is constructed following the design as in Section 2.1. To compare the properties with different materials as reinforcements, here we adopted the same size parameters for steel bar and GFRP, only the adopted material property changes for different cases. To study the effect of different amounts of reinforcement, a ranging spacing is considered for both reinforcement materials, which is shown as ΔL in Fig. 2c and ranges from 6-12 in.
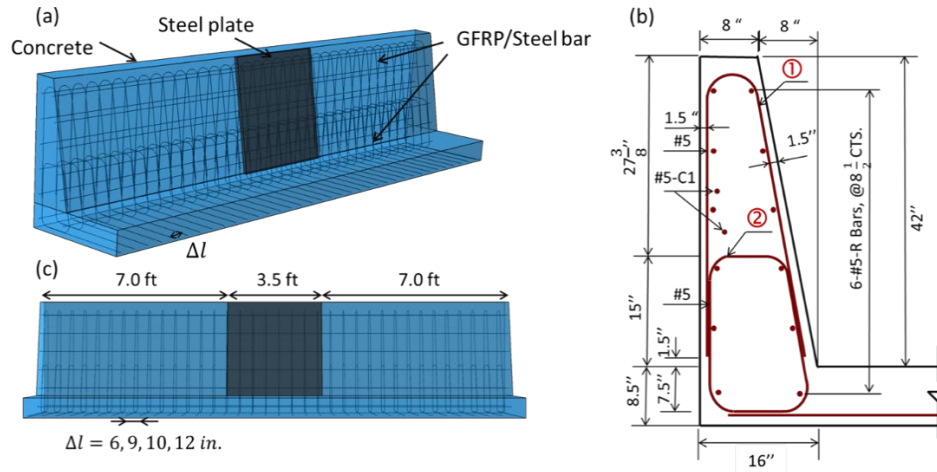
Figure 2 (a) GFRP/steel reinforced concrete barrier model construction. (b) GFRP/steel reinforcements. (c) Size parameters.

To take the casting techniques into consideration, we built 2 different concrete barrier models. The first class of barriers are well connected to the base to model the concrete barriers casted along with the bridge deck. The second class of barriers are constructed separated with the bridge deck to model the barriers that are separated casted in different steps, where the contact surfaces are set to be rigid contact and the connection is mainly contributed by the reinforcement. Based on these considerations, a total of 4 series of cases are designed and modeled, each with different reinforcement materials and model constructions, as shown in Tab. 1. Each series contains 4 cases with different reinforcement spacing (ΔL). The concrete part is meshed with 8-node linear 3D solid elements assigned with homogeneous material properties. The reinforcements, including steel bar and GFRP bars, are modeled with 1D truss elements and embedded into the concrete model using non-sliding setups.

Table 1 Cases setup

	Whole *	Separated **
Reinforced with *GFRP*	GFRP-1	GFRP-2
Reinforced with *steel bar*	Steel-1	Steel-2

8

*: the concrete barrier is casted with the bridge deck.

**: the concrete barrier is separately casted.

The static loading condition is applied on the barrier via a steel plate, as shown in Fig. 2a. The length of the steel plate is set as 3.5 ft, according to AASHTO LRFD Bridge Design Specifications, which is also 1/5 of the barrier model length. TL-4 test level is adopted here for the parameter setups. To make it valid for all types of vehicles and the center of mass location varies for different type of vehicles, for general consideration, fully coverage is considered along the height of the barrier. Displacement-controlled loading is considered. The material properties for concrete, steel and GFRP are included in Table 2-4. The stress-strain relationships of the materials are shown in Fig. 3. Note that the strength degradation effect of bending is considered by adopting the strength reduction factor specified in code ACI 440 [28].
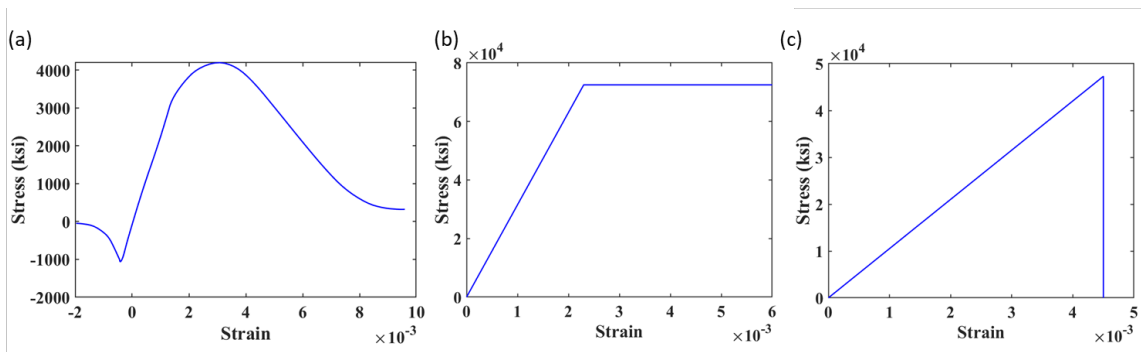

Figure 3 Material properties for (a) concrete, (b) steel and (c) GFRP.

Table 2 Concrete material property

Dilation angle	31	Density (kcf)	0.150
Eccentricity	0.1	E (ksi)	3644
fb0/fc0	1.16	v	0.2
K	0.67	f'c (ksi)	4.0
visco	0		

9

Table 3 Steel bar material property

Density (lb/ft³)	490.75
E(psi)	2.90E+7
v	0.26
Strength (Pa)	6.89E+4

Note: ASTM A36 steel bar for general structural purposes including bridges and buildings is considered for property determination.

Table 4 GFRP material property

Density (lb/ft³)	112.37
E(psi)	1.05E+7
v	0.33
Strength* (psi)	4.73E+4

* GFRP strength has been adjusted based on the strength reduction factor specified in ACI 440 [28].

2.2.2 Modeling Results

The stress distribution and concrete damage distributions for representative cases of all series are shown in Fig. 4-11. For different concrete cast scenarios with same kind of reinforcements, the failure patterns have significant differences. Comparing Fig. 4 & 5 with Fig. 6 & 7, for the GFRP-1 series where the concrete barrier is constructed as one whole part, the concrete damage mainly appears on the upper parts of the barrier and the damaged zone has a 45-degree angle with the horizontal line. This is consistent with the direction of the first principal stress and indicates the beginning of the softening stage. Moreover, stress concentrations as well as concrete yield domains with lower values are also observed around the junction between the barrier and the bridge deck,

which contributes but does not dominate the failure process. The stress distribution of the reinforcement (GFRP) is also consistent with this behavior, where the maximum stress is mainly distributed close to the front side where the impact force is applied.

As for the GFRP-2 series where the concrete barrier and bridge deck are constructed as 2 separate parts, the damage mainly occurs around the junction of these 2 parts while the concrete barrier is observed with minor yields. The strength of this group of concrete barriers is controlled by the structural behavior and depends on the strength of the conjunction. Correspondingly, seen from the stress distribution of the reinforcements as shown in Fig. 7, the maximum stress mainly appears around the back side as well as the junction of two concrete parts. This trend is also observed from the comparison between steel-1 and steel-2 series of cases (Fig. 8-9 with Fig. 10-11), the failure of steel-1 cases is mainly controlled by the material property while the failure of steel-2 cases is a combination of material properties as well as structural behavior.

As a summary, the GFRP reinforced concrete barriers have similar damage patterns as the steel reinforced ones, the adoption of different reinforcement materials doesn't alter the failure mechanism of the concrete barriers. The main failure mode is the concrete crushing near the loading region. The "yield-line" type failures were observed for the cases where the barrier was connected with the deck to simulate the monolithic casting. For the cases where the barrier was disconnected with the deck, the maximum stresses shifted to the back of the stirrup 1 reflecting the additional rotation at the barrier-deck joint. Overall, the GFRP reinforced concrete barriers have a relatively lower stress in concrete due to the higher rigidity of the reinforcement.
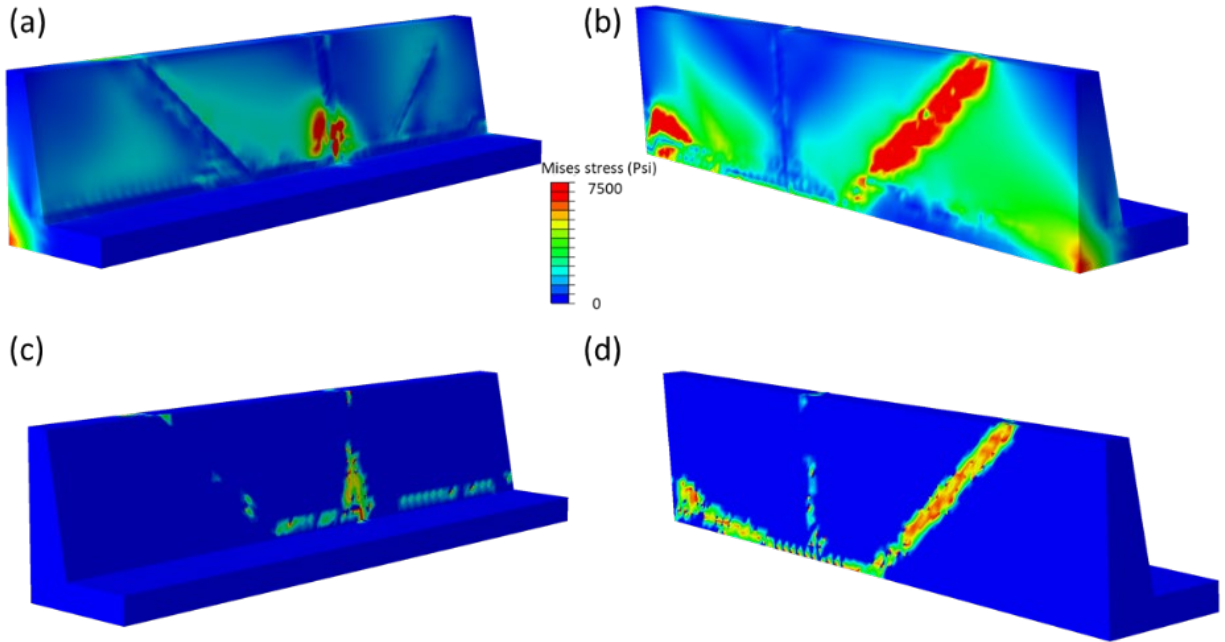
Figure 4 GFRP-1 series modeling results. (a-b) Stress distribution of front and back view of the barrier. (c-d) Yield distribution of front and back view of the barrier.

Figure 5 Stress distribution for reinforcements of GFRP-1 series.

Figure 6 GFRP-2 series modeling results. (a-b) Stress distribution of front and back view of the barrier. (c-d) Yield distribution of front and back view of the barrier.
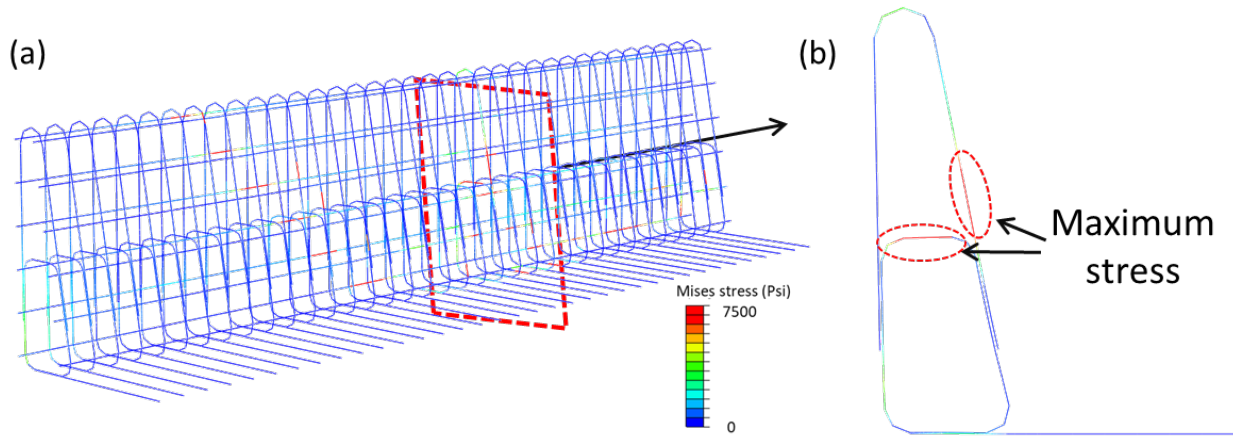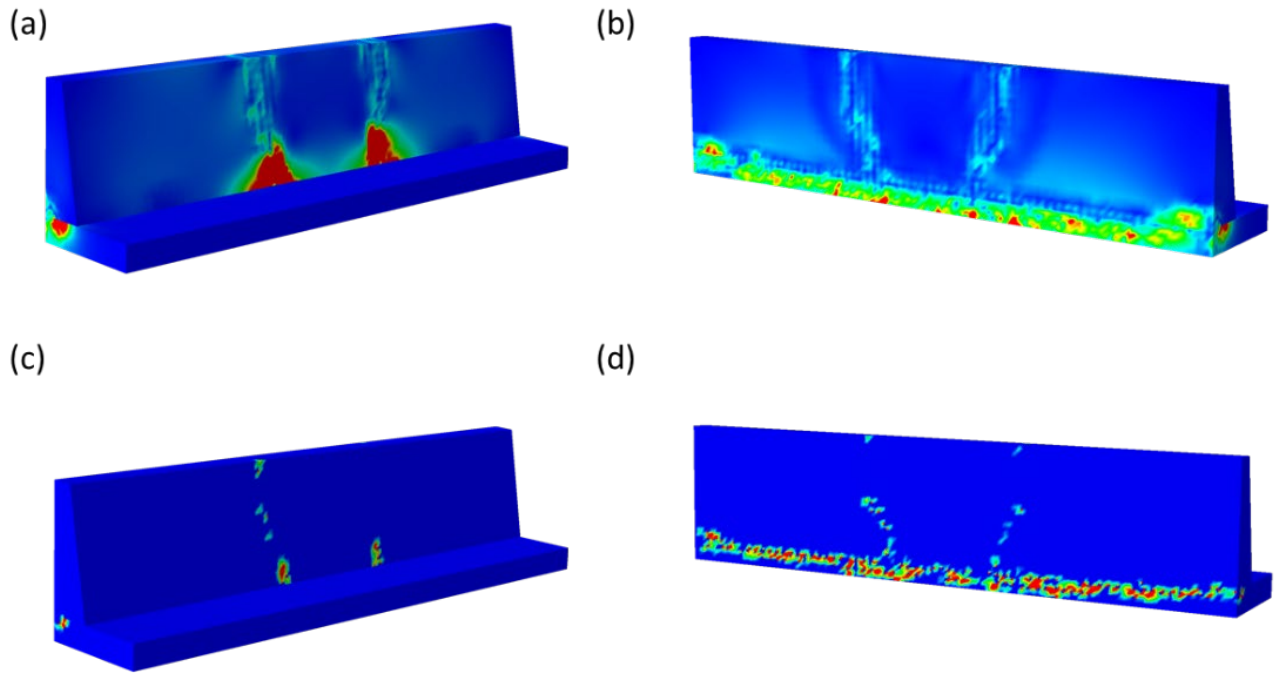

Figure 7 Stress distribution for reinforcements of GFRP-2 series.

Figure 8 Steel-1 series modeling results. (a-b) Stress distribution of front and back view of the barrier. (c-d) Yield distribution of front and back view of the barrier.

Figure 9 Stress distribution for reinforcements of steel-1 series.
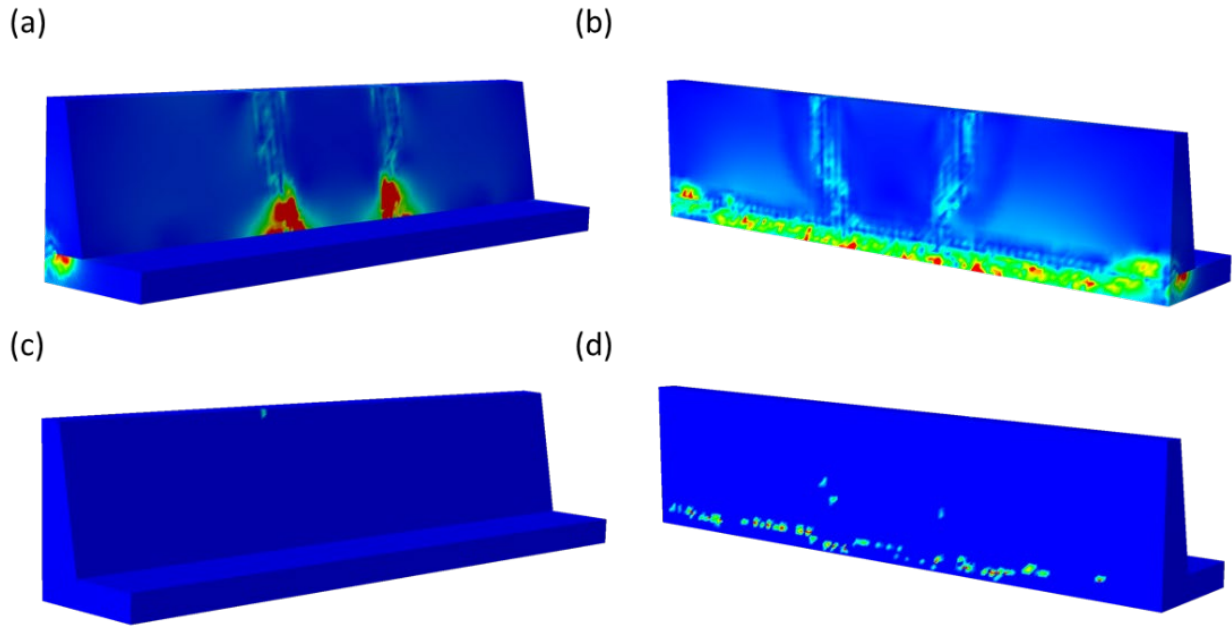
Figure 10 Steel-2 series modeling results. (a-b) Stress distribution of front and back view of the barrier. (c-d) Yield distribution of front and back view of the barrier.
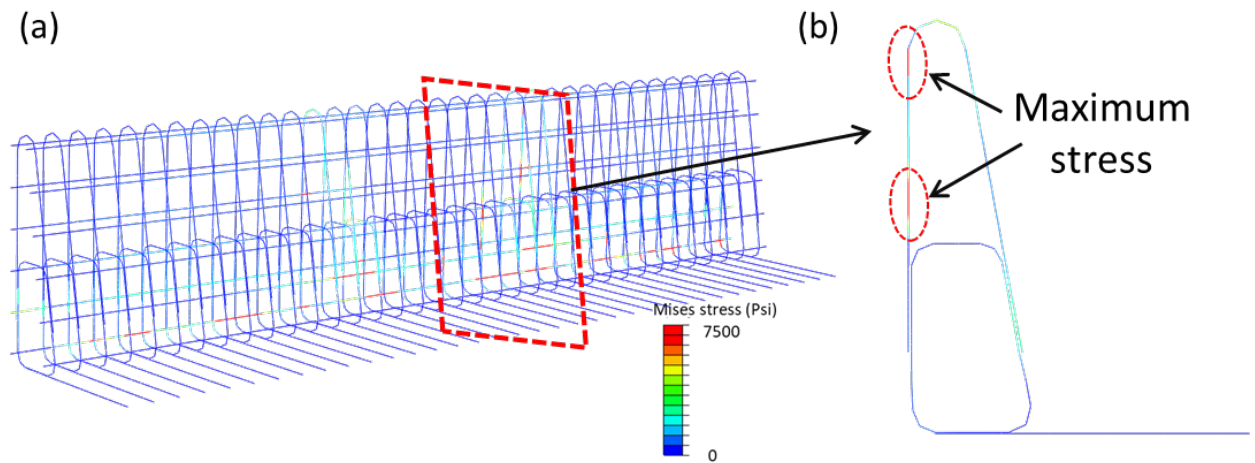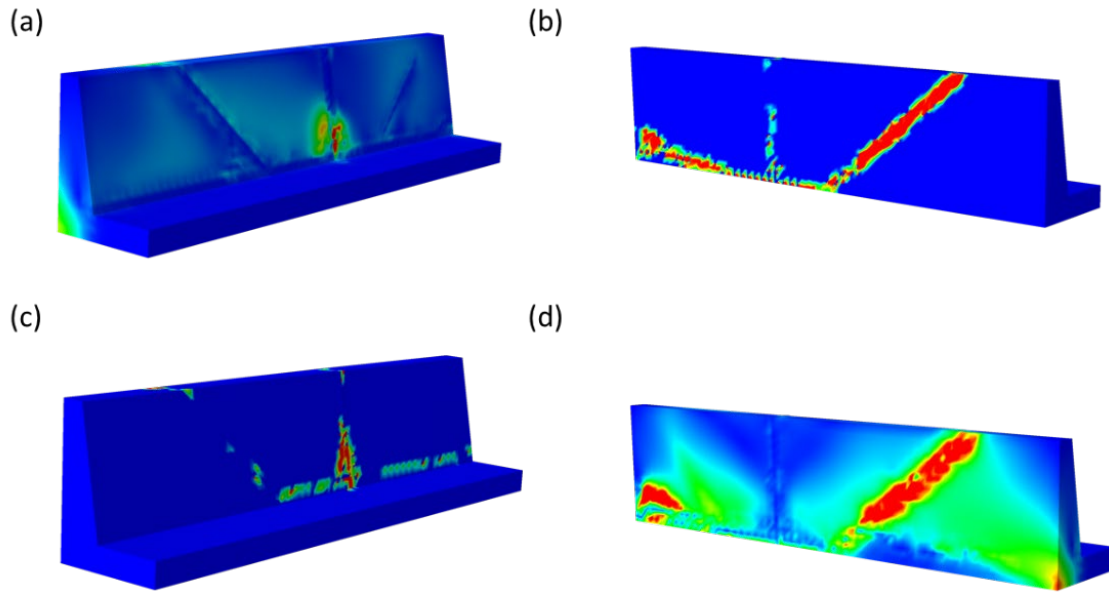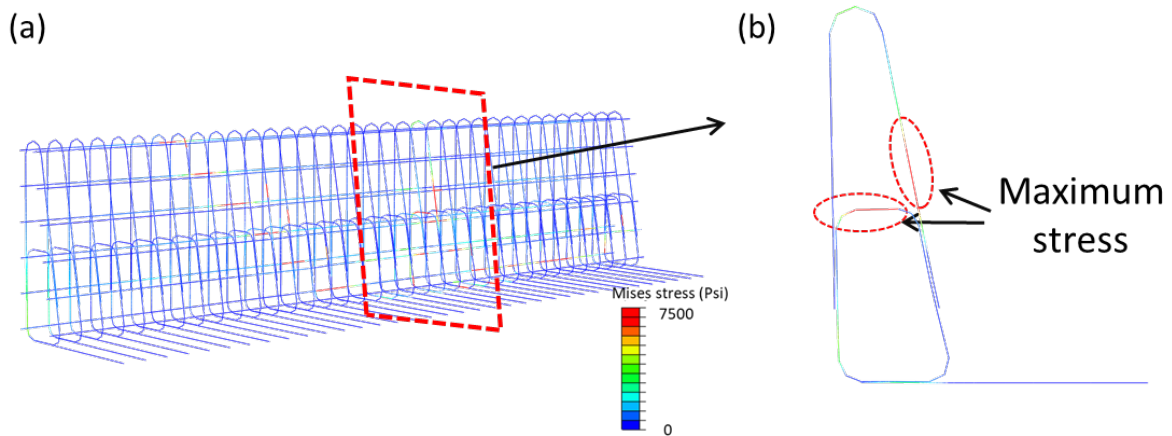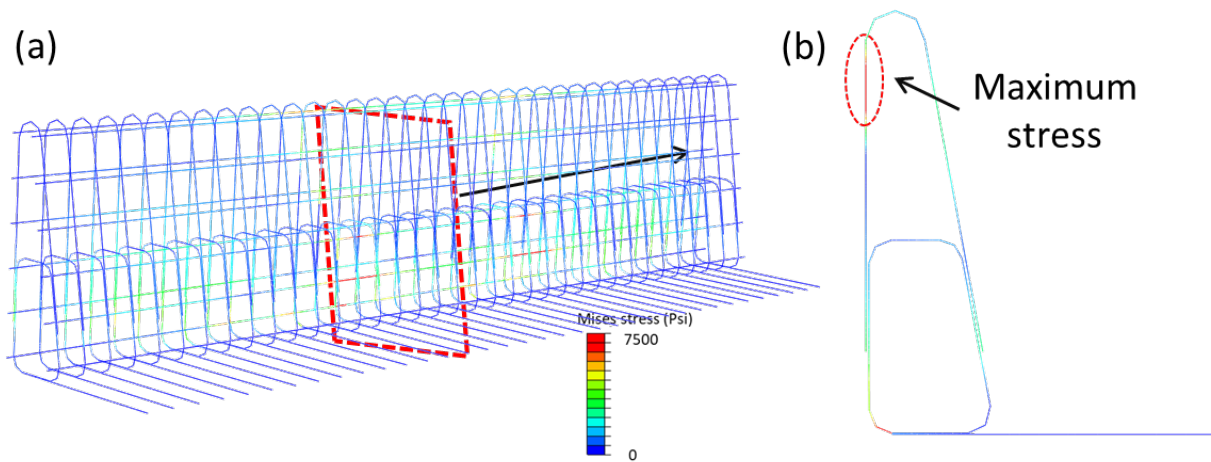

Figure 11 Stress distribution for reinforcements of steel-2 series.

The reaction force curves for all series of cases with ranging reinforcement spacing are shown in Fig. 12 while the strengths are shown in Fig. 13. From Fig. 12-13, the reaction force increases quasi-linearly with the loading progress at the beginning. Afterwards, the slope decreases, and the reaction force starts to decrease gradually after reaching the peak value (strength) until failure. The

15

cases with concrete barrier casted monolithically (GFRP-1 and steel-1 cases) have larger strengths than the cases where the concrete barrier and bridge deck are casted separately (GFRP-2 and steel-2 cases). The different reinforcement doesn't show significant influence in the strength as well as the trends of reaction forces. This is because the maximum stress of reinforcement (GFRP or steel) after the failure of concrete barrier is still much lower than the strength of the reinforcement. From Fig. 13, the strength is decreasing with the increasing spacing, due to the less reinforcements used in the barrier. It should be noted that this decrease effect caused by the changing spacing is very limited, which reflects in the small absolute differences between the strengths for all cases.
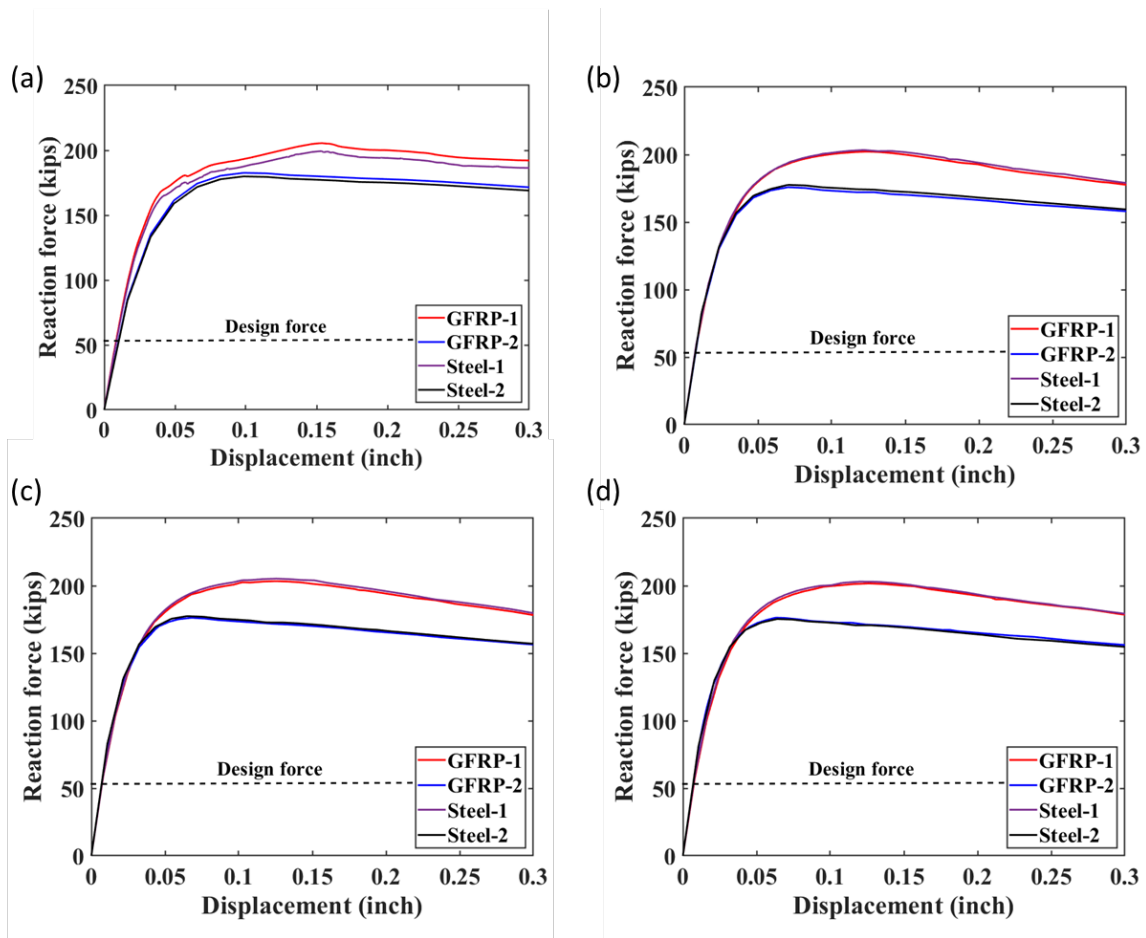

Figure 12 Reaction forces versus displacements for (a) $\Delta L = 6\ in$, (a) $\Delta L = 9\ in$, (a) $\Delta L = 10\ in$, (a) $\Delta L = 12\ in$.
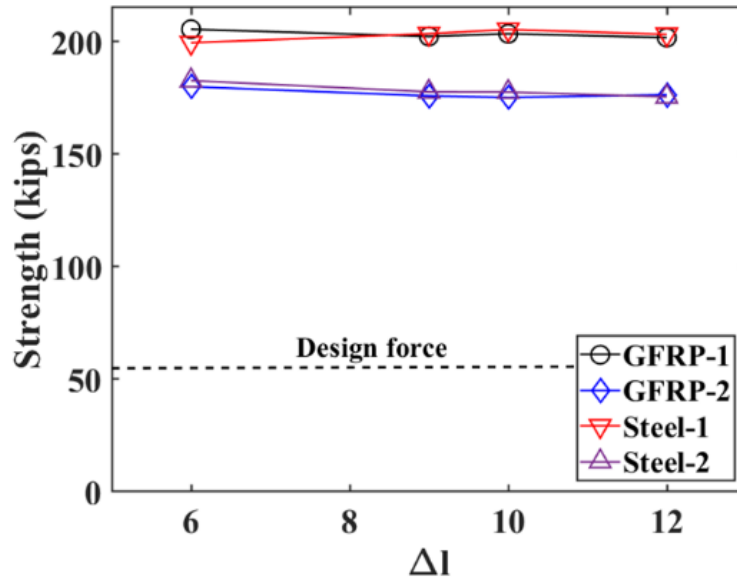
16

Figure 13 Strengths versus *ΔL* ft for both GFRP and steel reinforced concrete barriers

To sum, the strength of the GFRP reinforced concrete barriers have similar strengths as those reinforced with steel. The effects of stirrups space were found to be alike for both GFRP and steel reinforced concrete barriers. All barriers showed failure strength above 150 kips in terms of reaction forces, which are much higher than the design strength of 54 kips.

2.3 Behavior of GFRP Reinforced Concrete Barrier Under Dynamic Loading Conditions

This work aims to provide quantitatively analysis for the behavior of GFRP reinforced concrete bridge barriers that is under vehicle impact. To simulate the real scenarios, different impact angles are considered and modeled. Cases studied in this section are carried out with commercial software ABAQUS implicit and LS-Dyna. The main goal of using ABAQUS is to obtain a more detailed stress distribution in the structure since ABAQUS has a more enriched non-linear analysis function. However, due to the high computational cost, only 90-degree impact modeling were conducted in ABAQUS to provide guidance for the subsequent varying angle impact modeling performed in LS-Dyna.

17

2.3.1 Car Impact Modeling Using ABAQUS

The car impact model is shown in Fig. 14. To avoid excessive computation, only the front part of the car is considered and constructed with shell elements. Frontal collision is considered in this case. To make the model able to simulate the real cases, the density of the car shell elements is set to be larger than real aluminum materials so that the shell could have a self-weight comparable to a real car. An initial velocity of 60 mph is considered for the car while the barrier is totally fixed on the lower boundary.

The modeling results are shown in Fig. 15-16 for the car as well as the concrete barrier. It can be observed that the car after impact has a large deformation on the front and lower parts, which are also the locations of stress concentrations. Meanwhile, the barrier has shown limited deformations. The maximum stress is located at the contact point with the car, as expected. The influence of this impact on the deformation and damage of the nearby area is very limited. The reaction force from this impact has a maximum value of 31.77 kips, which is much lower than the strength of the concrete barrier calculated in Section 2.2.
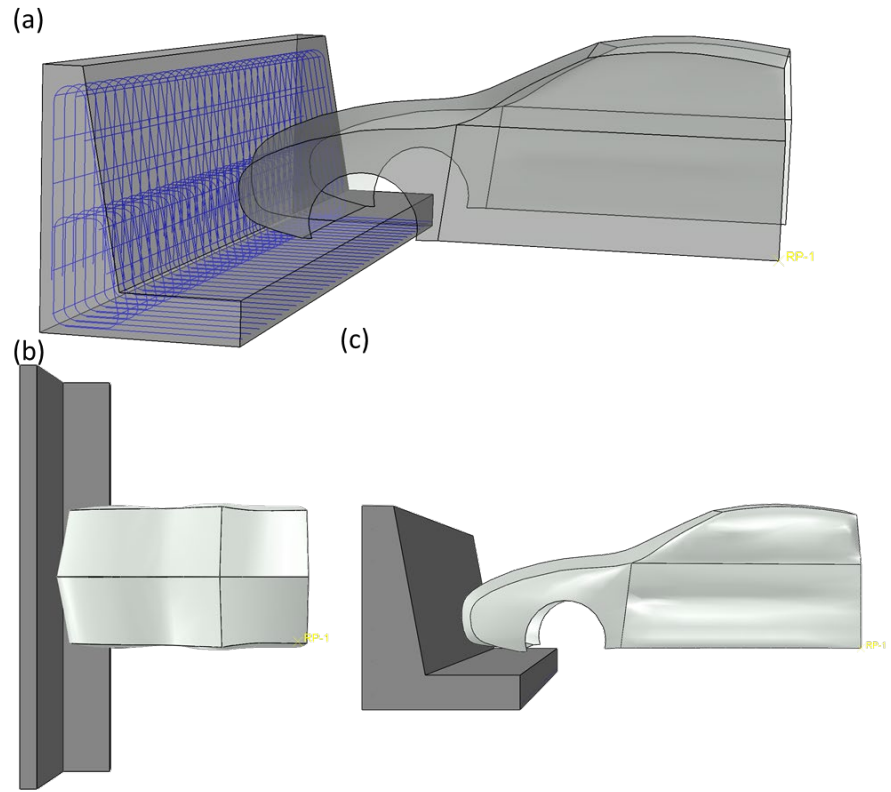
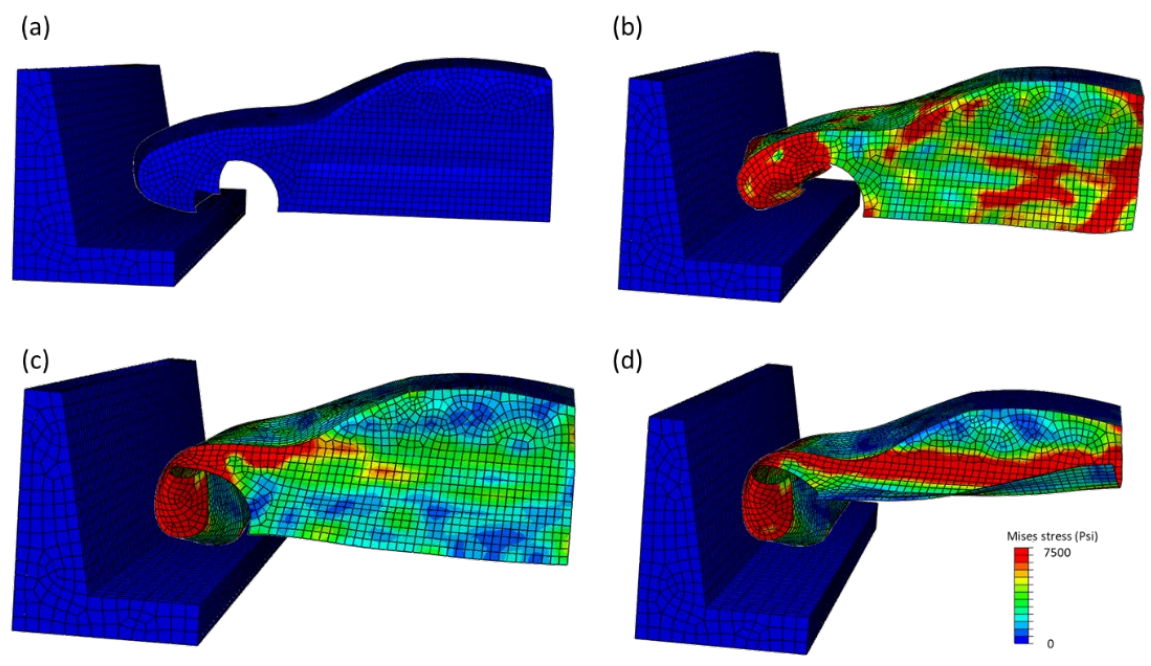**Figure 14 (a-c) Normal, top and front view of the 3D model.**
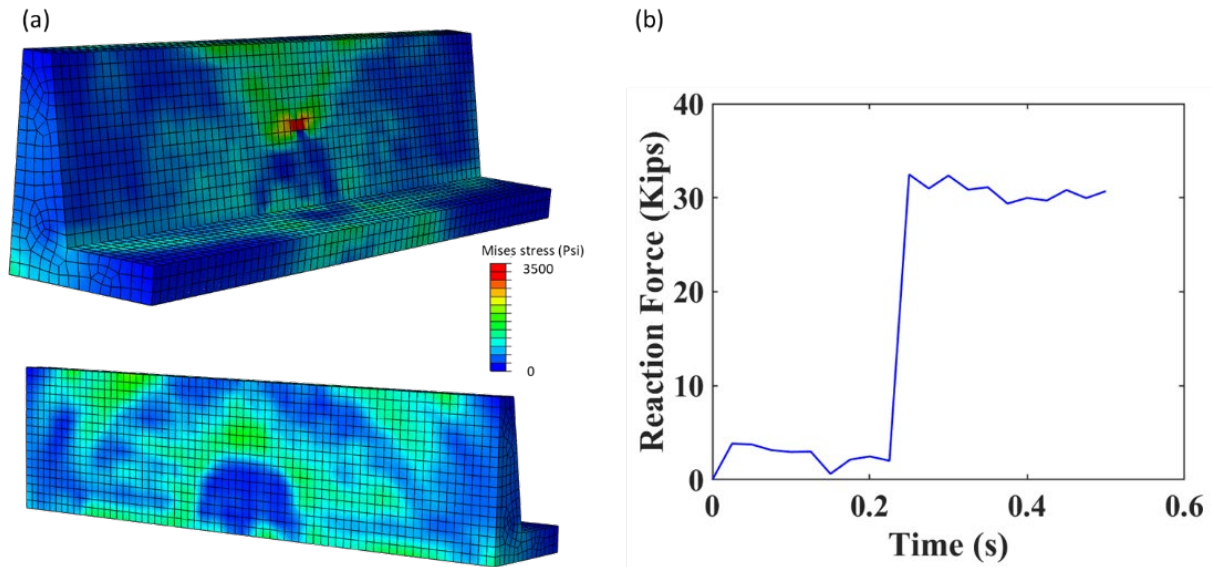

Figure 15 Car crash procedure.

Figure 16 (a) Stress distribution of the concrete barrier. (b) Reaction force development.

2.3.2 Truck Impact Modeling Using ABAQUS

Following the similar procedures, the impact of a truck on the concrete barrier is also conducted using ABAQUS implicit. Truck shell model is constructed where the density is set to be larger to meet the self-weight of a real-world truck. The initial velocity is also set as 60 mph. The modeling results are shown in Figs. 18-19.

With the height of the truck larger than the height of the concrete barrier, it is mainly the lower part of the truck that is deformed and has the stress concentration. Due to the flat surface, the contact area between the truck and the concrete barrier is larger than that of the car impact, which results in multiple points stress concentration shown in the Fig. 19. It can also be observed that the stress distributed on the back of the barrier is much lower than that of the front. This indicates that the impact load applied on the barrier is well dispersed to the whole barrier structure rather than one specific part and avoids the damage that might be caused by this impact. Moreover, this is also reflected as a lower maximum value but relatively long platform in the reaction force curve. Also,

20

the maximum reaction force for the truck impact is also much lower than the strength of the concrete barrier calculated in Section 2.2.
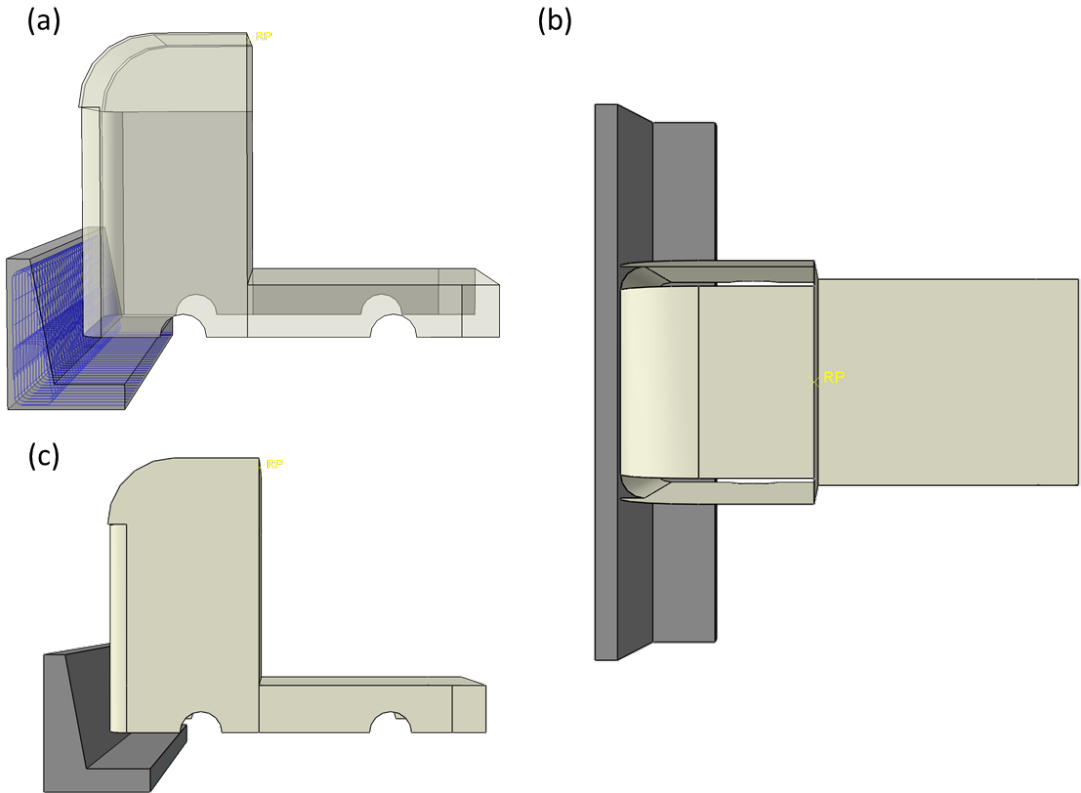
(a)

(b)

(c)

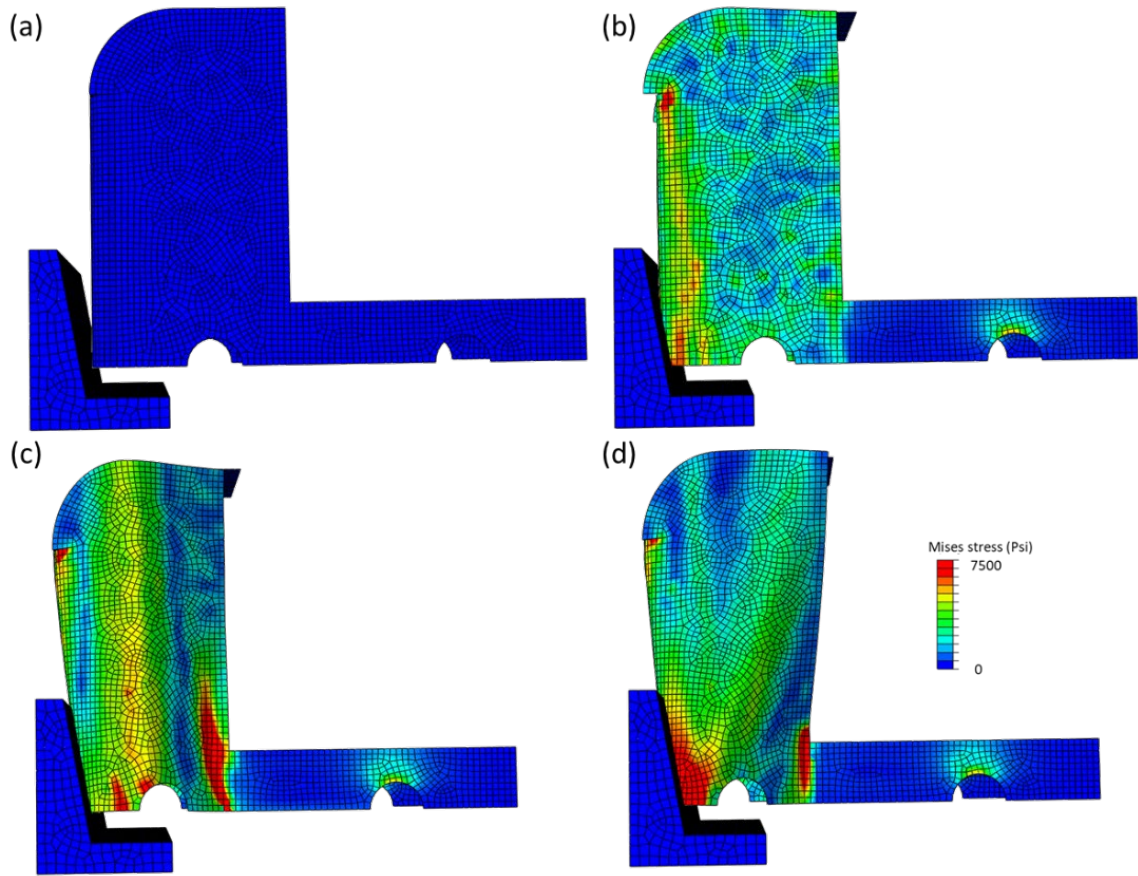**Figure 17 (a-c) Normal, top and front view of the 3D model.**

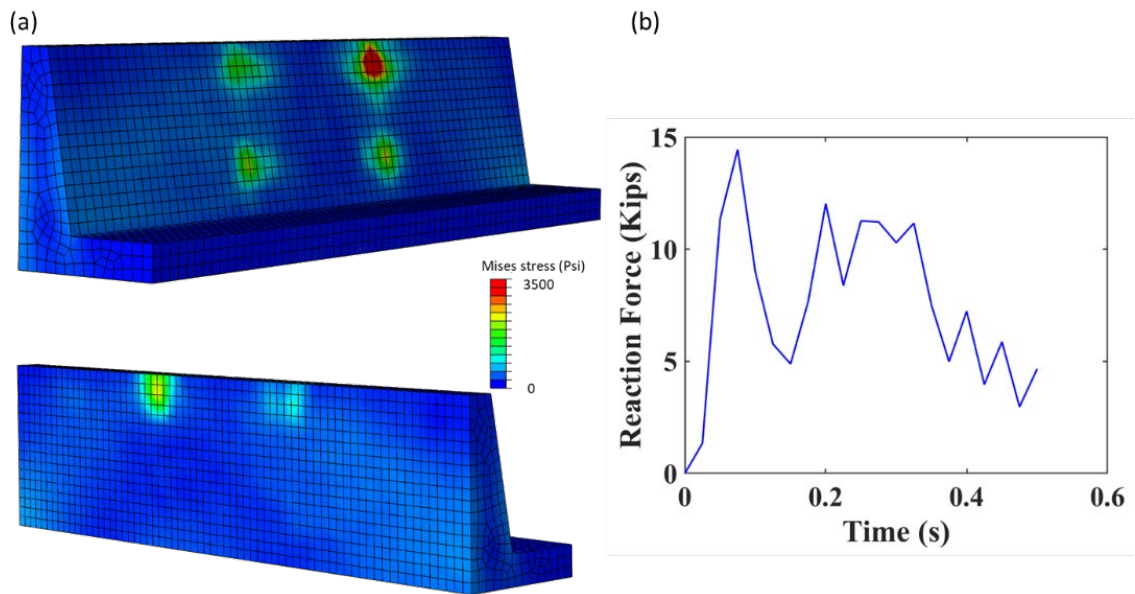**Figure 18 Truck crash procedure.**

Figure 19 (a) Stress distribution of the concrete barrier. (b) Reaction force development.

From the ABAQUS modeling results, we have found that most of the impact energy went into the vehicle due to the relatively high non-linear responses of the vehicle structures. However, it is suspected that the shell elements used in the model could lead to artificial compliances. In addition, the excessive computation cost involved using ABAQUS makes it challenging to model varying angle impact. Therefore, LS-Dyna modeling was further conducted, which will be explained in the following section.

2.3.3 Truck Impact Modeling Using LS-Dyna

In this section, a truck impact case is modeled using LS-Dyna. Referring to the MASH standard [29], a C1500 pick-up truck model that is weighted around 5000 pounds is constructed based on one online model as shown in Fig. 20. 4 different crash cases with different impact angles are modeled to simulate different impact scenarios. Other than the recommended 25-degree impact angle, we considered a total of 4 ranging impact angles to verify the feasibility and safety of the GFRP reinforced concrete barrier. In this work, the impact angle is defined as angles between the truck moving direction with the barrier and adopts 4 different values, $90, 67.5, 45, 22.5$.
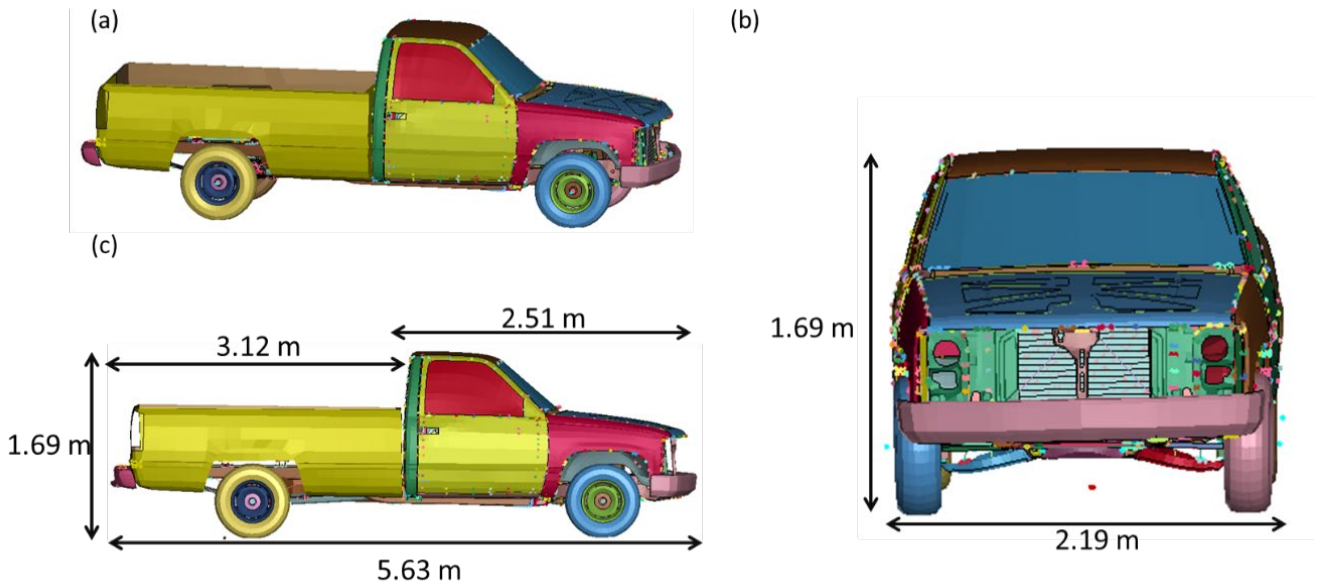
Figure 20 (a-c) Normal, front and side view of the 3D model.

Figure 21 Truck crash model setup.

Different truck parts are assigned with corresponding material properties and meshed with mass, beam, shell or solid element types that are provided by the LS-Dyna, depending on the shape and size of each part. The ground is modeled with 4 rigid walls, each set for a corresponding wheel. As for the concrete barrier, the concrete part is meshed with mass elements and assigned with

concrete damage plastic model, the GFRP reinforcement beam elements are assigned with anisotropic plastic property and embedded into the concrete structure.

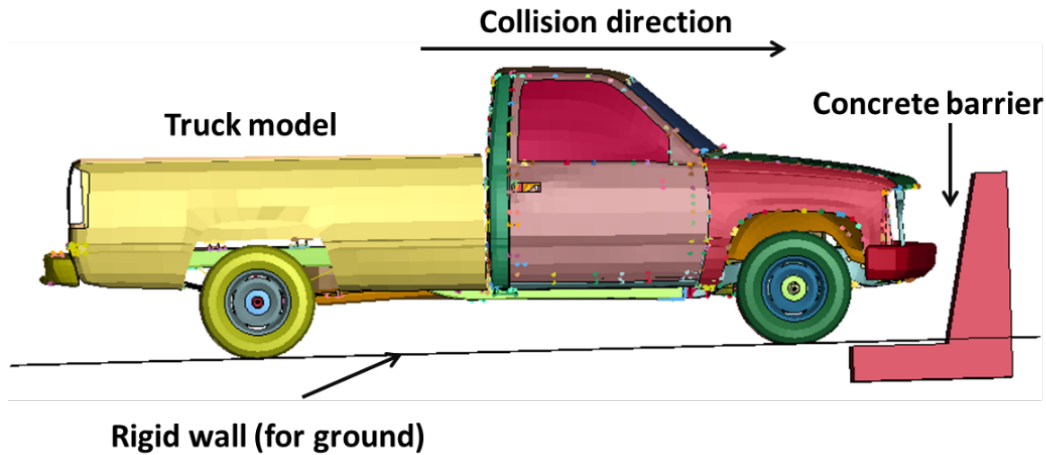The truck is assigned with an initial velocity of 62 mph at the moment of collision, which is based on the TL-4 rating for pick-up trucks. The GFRP reinforced concrete barrier is totally fixed on the lower boundary.

The modeling results for each of 4 cases are shown in Fig. 22-33. Seen from the collision procedures as well as the stress distributions, the difference of the impact angles directly reflects in the failure modes of truck as well as the GFRP reinforced concrete barrier, which is also reflected in the reaction force curves.

For all cases, the stress concentration happens mainly on the front part of the truck. The front part is observed with large deformation and damage while the latter part of the truck is with much smaller level of deformations. Comparingly speaking, the GFRP reinforced concrete barrier is barely deformed or damaged. This verifies that the GFRP reinforced concrete barrier design meets the requirement specified by the MASH standards.

As for pick-up trucks in different impact angle cases, it can be observed that the level of damage decreases with the decreasing impact angle. For the cases with relatively larger impact angles (90 and 67.5), the front part of the truck is severely damaged. Comparingly, in the cases with relatively smaller impact angles (45 and 22.5), only part of the truck is deformed, and the damage level is much lower.

The stress distribution pattern in the GFRP reinforced concrete barrier also changes with the impact angle. For the cases with relatively larger impact angles (90), the maximum stress mainly develops on the upper part of the barrier around the impact location. As for the cases with smaller impact angles (67.5, 45 and 22.5), the maximum x-direction stress is developed around the junction between the barrier and the bridge deck, the impact load is well dispersed to the whole barrier.

This is due to the different time period from first contact to the final failure that is caused by different impact angles. For cases with large impact angle (90), the buffer for collision is very limited and the dynamic energy is released in a very short time. This causes the severe damage observed on the truck as well as the stress concentrated on the upper part of the barrier. Comparingly speaking, smaller impact angles lead to a larger buffer zone before final failure, this answers for the slighter damage observed on the trucks of smaller impact angle cases as well as the stress concentration around the junction.

This is also observed in the reaction forces curves for all cases. Although most of the reaction forces follow an increasing-decreasing 2 stage behavior, the peak point appears relatively earlier for cases with larger impact angles. This is consistent with the smaller buffer zone in these cases.
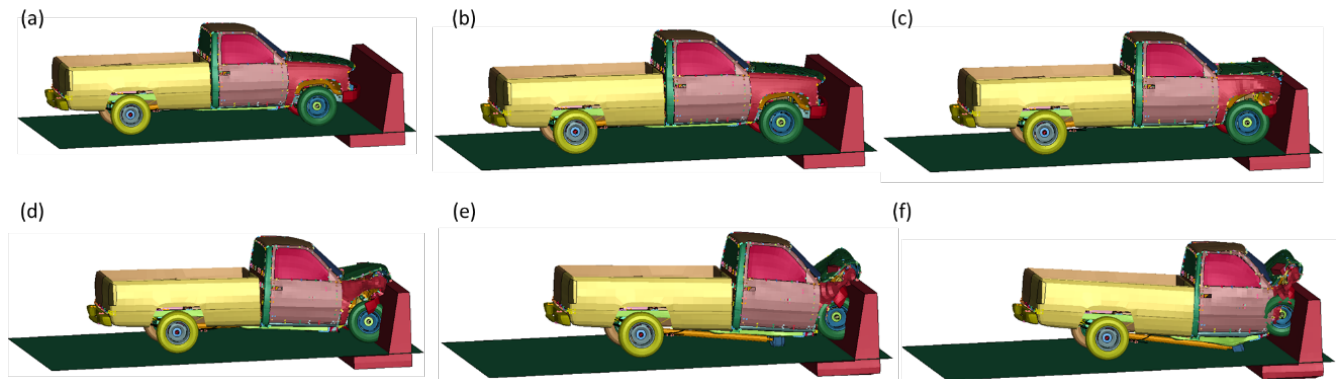

Figure 22 Truck crash procedure with impact angle being 90.

Figure 23 (a-b) First principal stress distribution. (c-d) x-direction stress distribution. Stress unit: MPa

Figure 24 (a-b) X- and y-direction reaction forces with impact angle being 90.

Figure 25 Truck crash procedure with impact angle being 67.5.

Figure 26 (a-b) First principal stress distribution. (c-d) x-direction stress distribution. Stress unit: MPa

Figure 27 (a-b) X- and y-direction reaction forces with impact angle being 67.5.
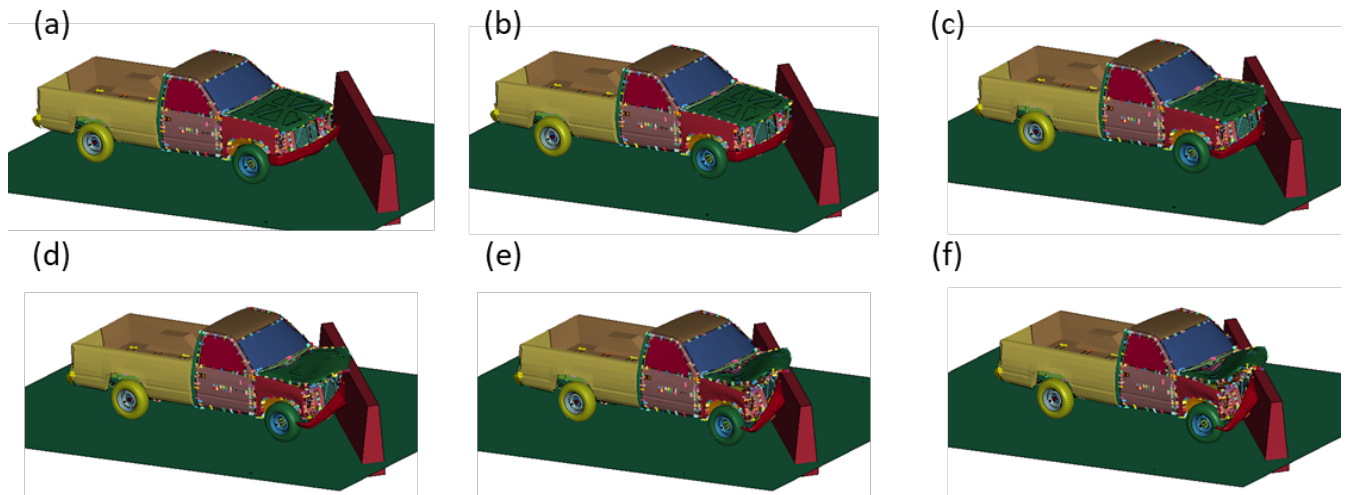
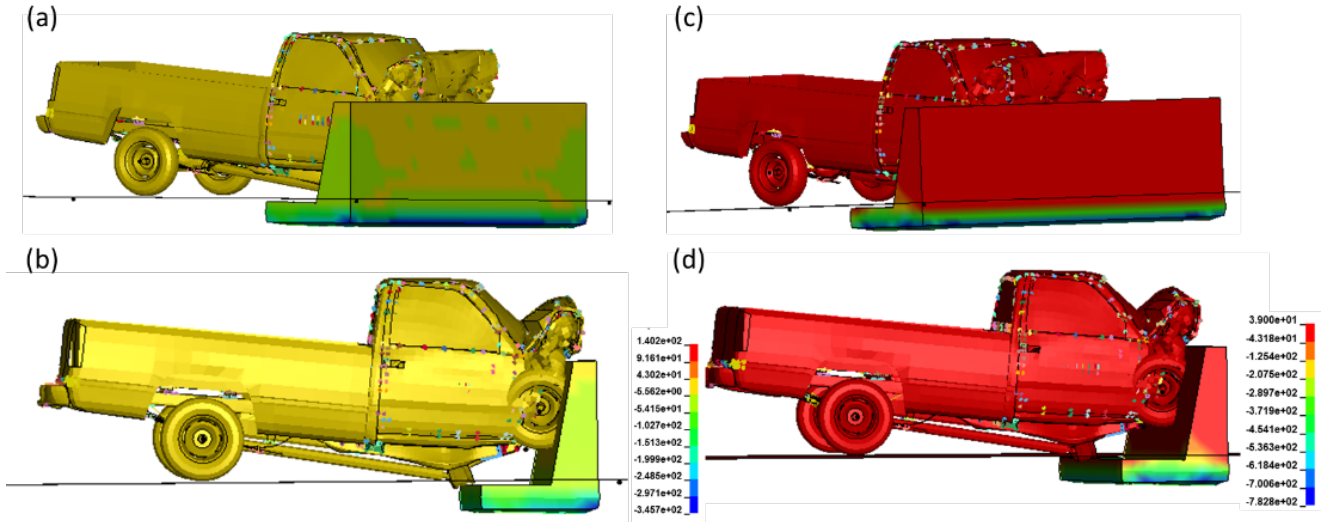**Figure 28 Truck crash procedure with impact angle being 45.**
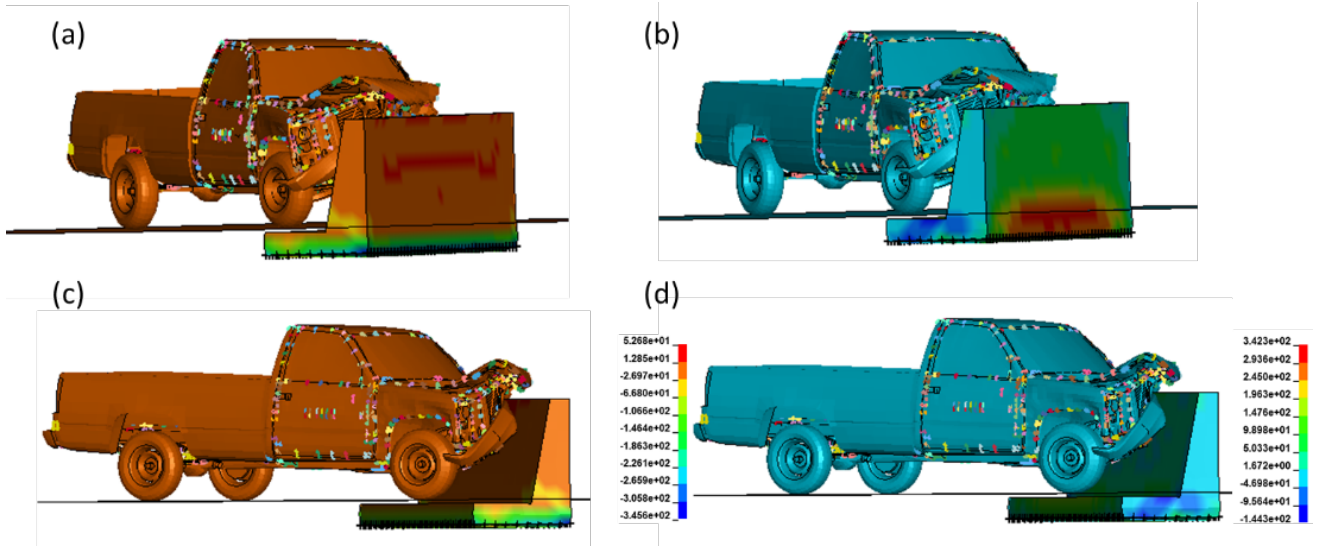
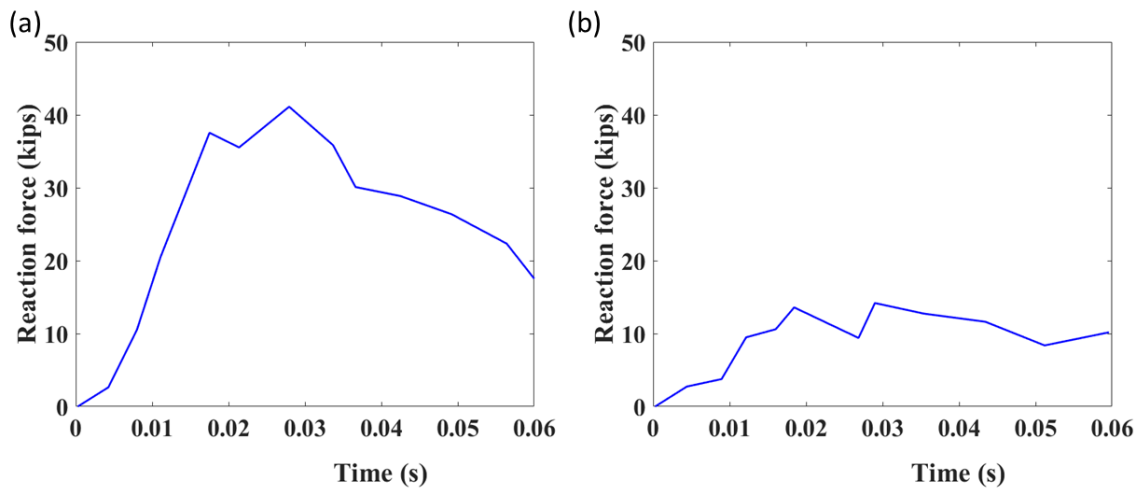**Figure 29 (a-b) First principal stress distribution. (c-d) x-direction stress distribution. Stress unit: MPa**
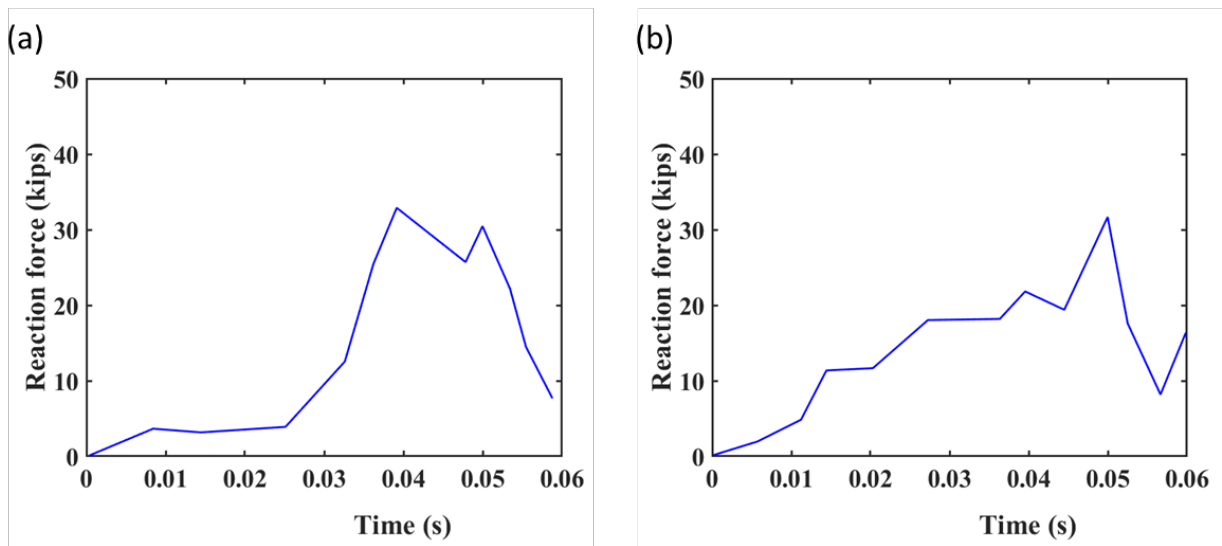
Figure 30 (a-b) X- and y-direction reaction forces with impact angle being 45 degree.
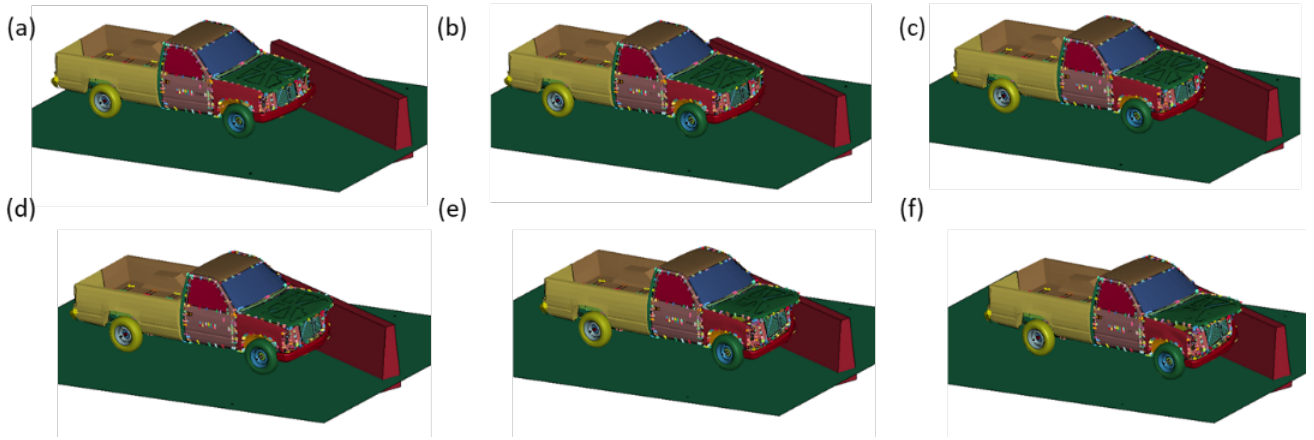
Figure 31 Truck crash procedure with impact angle being 22.5 degree.
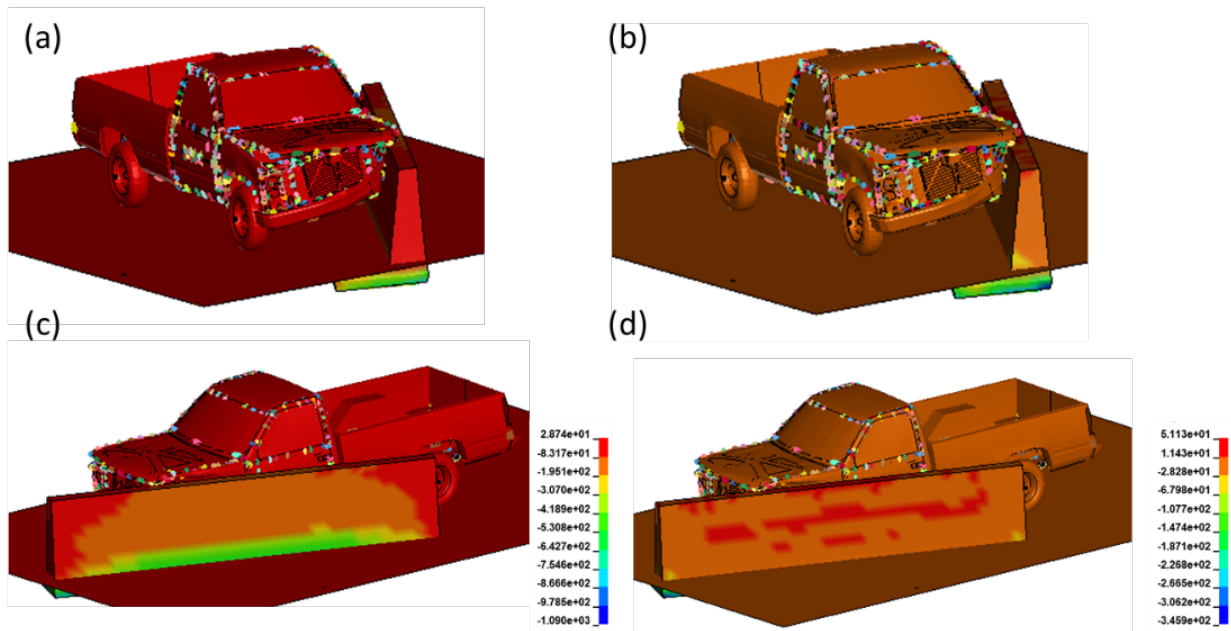
Figure 32 (a-b) First principal stress distribution. (c-d) x-direction stress distribution. Stress unit: MPa

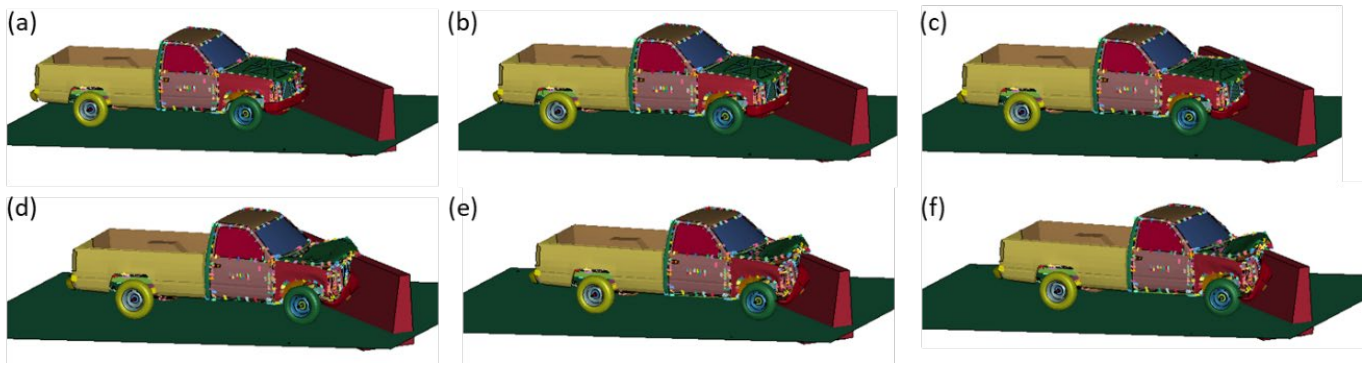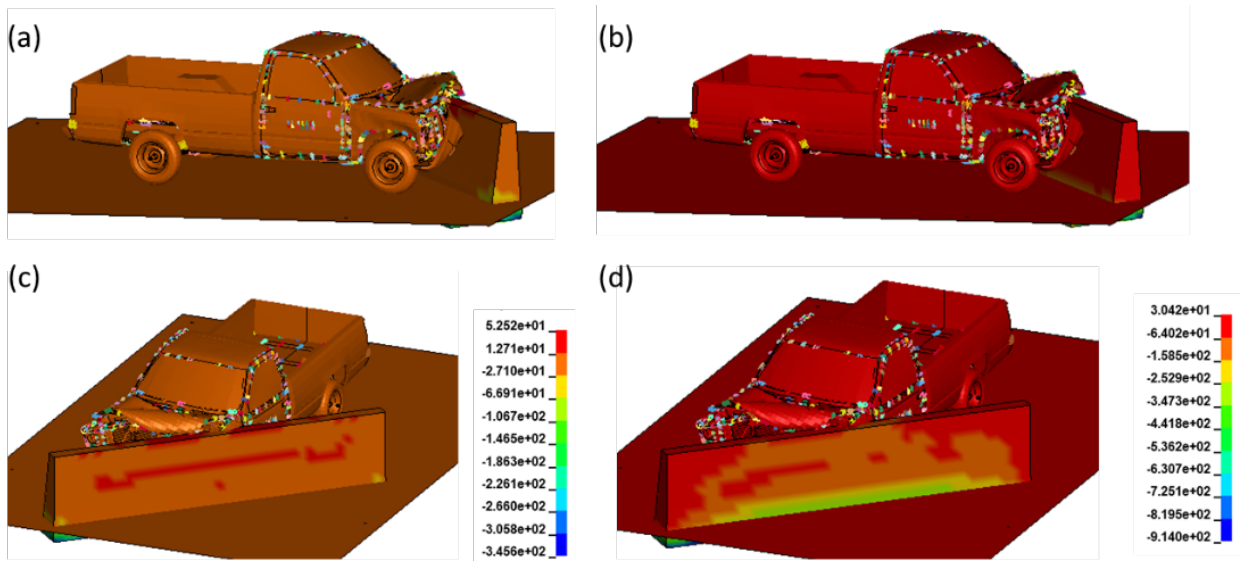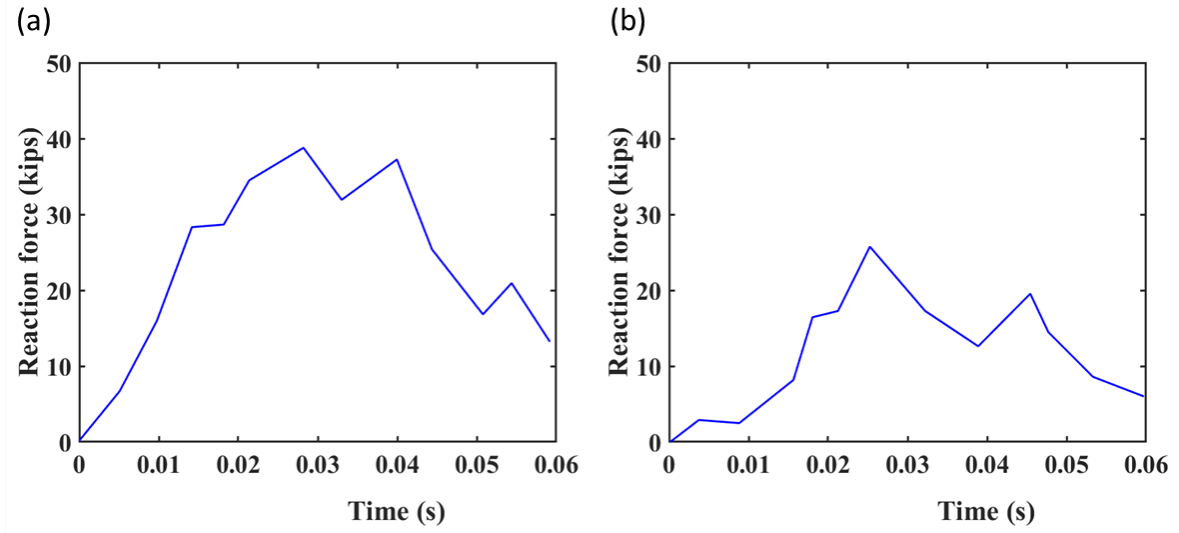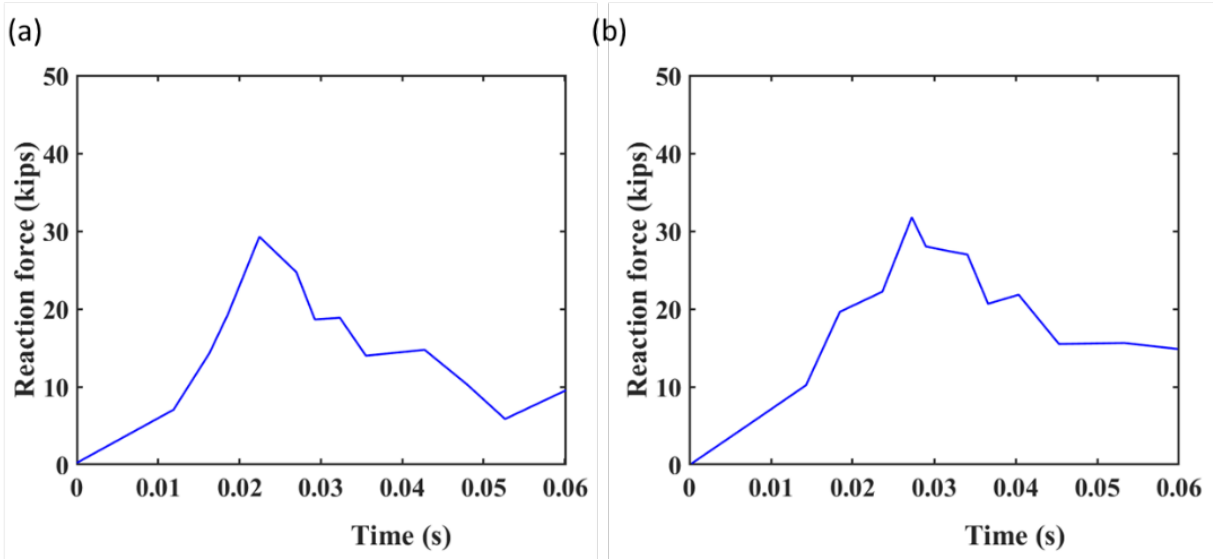**Figure 33 (a-b) X- and y-direction reaction forces with impact angle being 22.5.**
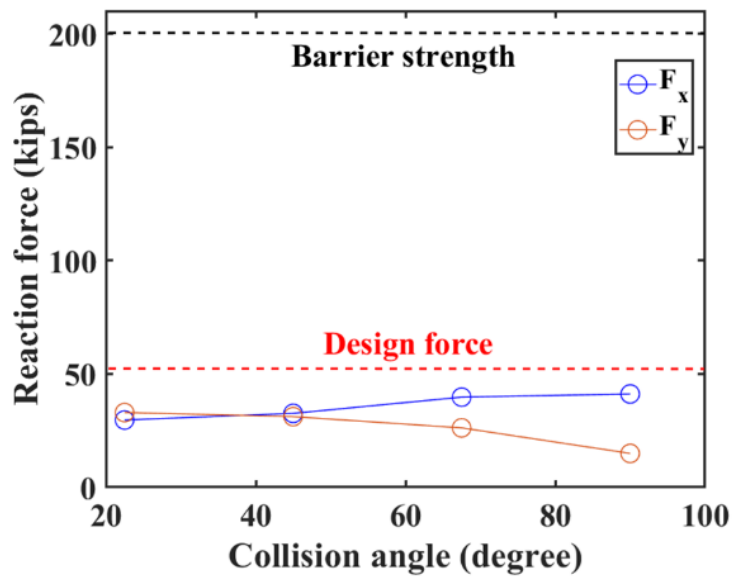
Figure 34 Maximum reaction force with respect to the impact angle.

Seen from Fig. 34, with the impact angle increasing, the maximum reaction force along x-direction is increasing and reaches the peak value at 90-degree impact angle. Meanwhile, the y-direction reaction force decreases. For all cases, the maximum reaction forces are much lower than the barrier strength obtained in Section 2.2.

3. CONCLUSIONS

This study on GFRP reinforced concrete barriers has successfully designed the GFRP reinforced concrete barrier that can be used for bridge structures. The behavior of this GFRP reinforced concrete barrier under static and dynamic loadings are numerically studied using commercial software ABAQUS and LS-Dyna.

For GFRP reinforced concrete barrier under static loading conditions consistent with the AASHTO specifications, modeling results reveal the following conclusions:

1. The model with concrete barrier casted along with the bridge deck (shown as a whole) could provide higher strength, comparing with the model where the concrete barrier is just partially connected to the bridge deck.

2. Different reinforcement material (GFRP and steel) does not have significant influence on the overall behavior and failure of the concrete barrier.

3. Less spacing between reinforcements could increase the overall strength with a limited effect.

4. Failure strengths of all cases, as presented in Tab. 5, are above 150 kips in terms of reaction forces, which are much higher than the design strength of 54 kips.

Table 5 Concrete barrier strengths (kips)

	$\Delta L = 6\ in$	$\Delta L = 9\ in$	$\Delta L = 10\ in$	$\Delta L = 12\ in$
GFRP-1	205.4	202.2	203.4	201.7
GFRP-2	179.9	175.8	175.1	176.3
Steel-1	199.4	203.4	205.3	203.1
Steel-2	182.6	177.6	177.5	175.4

For GFRP reinforced concrete barrier under impact load where the pick-up truck model construction and loading conditions adopted from MASH standards, modeling results reveals following conclusions:

1. The maximum stress as well as the damage is mainly observed on the truck instead of the barrier.

2. Peak reaction forces, as presented in Tab. 6, observed in all cases with different impact angles ranges from 15 – 45 kips. This is lower than the designed strength (54 kips).

3. Impact angle has influence on the x- and y- direction reaction force distributions as well as the emergence of the peak force.

4. No significant failure or deflection of the barrier is observed in any case, which satisfies the requirements of the MASH TL-4 standards.

Table 6 Peak reaction force (kips) versus impact angle

Collision angle (°)	22.5	45	67.5	90
F_x (kips)	29.69	32.61	39.77	41.15
F_y (kips)	32.97	31.18	26.22	14.97

Overall, the modeling results show that the design of the GFRP reinforcement satisfies the requirements of AASHTO and MASH standards. The laboratory testing is recommended to verify the modeling results.

4. REFERENCES

1. Ross Jr, HE, DL Sicking, Richard A Zimmer, and Jarvis Dale Michie, *Recommended procedures for the safety performance evaluation of highway features*. 1993.
2. Esfahani, Elham Sahraei, Dhafer Marzougui, and Kenneth S Opiela, *Safety Performance of Concrete Median Barriers under Updated Crashworthiness Criteria*. 2008, Citeseer.
3. Dhafer, M, M Buyuk, and S Kan, *Performance evaluation of portable concrete barriers. National Crash Analysis Center, The George Washington University*. 2007.
4. Sheikh, Nauman M, Roger P Bligh, and Wanda L Menges, *Development and Testing of a Concrete Barrier Design for Use in front of Slope or on MSE Wall*. 2009, Report 405160-13-1. Texas Transportation Institute, College Station.
5. Jeon, Se-Jin, Myoung-Sung Choi, and Young-Jin Kim, *Ultimate strength of concrete barrier by the yield line theory*. International journal of concrete structures and materials, 2008. **2**(1): p. 57-62.
6. Sturt, Richard and Christina Fell, *The relationship of injury risk to accident severity in impacts with roadside barriers*. International Journal of Crashworthiness, 2009. **14**(2): p. 165-172.
7. Atahan, Ali Osman, *Effect of permanent jersey-shaped concrete barrier height on heavy vehicle post-impact stability*. International Journal of Heavy Vehicle Systems, 2009. **16**(1-2): p. 243-257.
8. Tondolo, F, *Bond behaviour with reinforcement corrosion*. Construction and Building Materials, 2015. **93**: p. 926-932.
9. Wei, Congjie, Charles S Wojnar, and Chenglin Wu, *Hydro-chemo-mechanical phase field formulation for corrosion induced cracking in reinforced concrete*. Cement and Concrete Research, 2021. **144**: p. 106404.
10. Angst, Ueli M, *Challenges and opportunities in corrosion of steel in concrete*. Materials and Structures, 2018. **51**(1): p. 1-20.
11. Zhu, Xingji and Goangseup Zi, *A 2D mechano-chemical model for the simulation of reinforcement corrosion and concrete damage*. Construction and Building Materials, 2017. **137**: p. 330-344.
12. Fernandez, Ignasi, Jesús Miguel Bairán, and Antonio R Marí, *Mechanical model to evaluate steel reinforcement corrosion effects on σ–ε and fatigue curves. Experimental calibration and validation*. Engineering Structures, 2016. **118**: p. 320-333.
13. Hong, Shuxian, Herbert Wiggenhauser, Rosemarie Helmerich, Biqin Dong, Peng Dong, and Feng Xing, *Long-term monitoring of reinforcement corrosion in concrete using ground penetrating radar*. Corrosion Science, 2017. **114**: p. 123-132.
14. Abolghasem, Alireza, Hossein Azimi, Khaled Sennah, and Ekaterina Tropynina. *Experimental study on bond behavior of GFRP group Anchorage*. in *Proc., CSCE Annual Conf*. 2013.
15. Buth, C Eugene, William F Williams, Roger P Bligh, Wanda L Menges, and Rebecca R Haug, *Performance of the TxDOT T202 (MOD) bridge rail reinforced with fiber reinforced polymer bars*. Rep. No. FHWA/TX-03/0-4138, 2003. **3**.
16. Charron, J-P, E Niamba, and Bruno Massicotte, *Static and dynamic behavior of high- and ultrahigh-performance fiber-reinforced concrete precast bridge parapets*. Journal of Bridge Engineering, 2011. **16**(3): p. 413-421.

17.   Wilson, EL and A Habibuallah, *Integrated structural analysis and design software SAP2000.* Computers and Structures, Inc. Berkeley, California. http://www.csiamerica.com, 2009.

18.   Association, Canadian Standards, *Canadian highway bridge design code (CHBDC).* CSA Standard S6-00, 2000.

19.   Association, Canadian Standards, *Commentary on CAN/CSA-S6-06, Canadian highway bridge design code (CHBDC).* 2006.

20.   El-Gamal, S, B Benmokrane, and S Goulet. *Testing of concrete bridge barriers reinforced with new glass FRP bars.* in *Proceedings of the 37th CSCE Annual Conference.* 2008.

21.   El-Salakawy, Ehab, Brahim Benmokrane, Radhouane Masmoudi, Frédéric Briére, and Éric Breaumier, *Concrete bridge barriers reinforced with glass fiber-reinforced polymer composite bars.* Structural Journal, 2003. **100**(6): p. 815-824.

22.   El-Salakawy, Ehab, Radhouane Masmoudi, Brahim Benmokrane, Frédéric Brière, and Gérard Desgagné, *Pendulum impacts into concrete bridge barriers reinforced with glass fibre reinforced polymer composite bars.* Canadian Journal of Civil Engineering, 2004. **31**(4): p. 539-552.

23.   No, Design Manual, *ISIS CANADA RESEARCH NETWORK.* 2007.

24.   Maheu, John and Baidar Bakht. *A new connection between concrete barrier walls and bridge decks.* in *Proceedings of the CSCE Annual Conference.* 1994.

25.   Matta, Fabio and Antonio Nanni, *Connection of concrete railing post and bridge deck with internal FRP reinforcement.* Journal of Bridge Engineering, 2009. **14**(1): p. 66-76.

26.   Bank, Lawrence C, Nestore Galati, Fabio Matta, Antonio Nanni, Michael G Oliva, Thomas E Ringelstetter, Spencer N Jones, Brian G Orr, and Jeffrey S Russell, *Development and Field Testing of an FRP Composite Bridge Deck Comprising of Guard Rail System for Bridge 1480230, Greene County, MO.* 2010, University Transportation Centers Program (US).

27.   Jing, Xishuang, Siyu Chen, Jiuzhi An, Chengyang Zhang, and Fubao Xie, *Thermoplastic Mandrel for Manufacturing Composite Components with Complex Structure.* Aerospace, 2021. **8**(12): p. 399.

28.   440, American Concrete Institute. Committee. *Guide for the Design and Construction of Structural Concrete Reinforced with FRP Bars: ACI 440.1 R-06.* 2006. American Concrete Institute.

29.   Officials, Transportation, *Manual for Assessing Safety Hardware, 2009.* 2009: AASHTO.